

Design of ring-sector-assisted PANDA ring-core few mode fiber*

DU Zhiyong, WANG Chuncan**, LI Peixin, PEI Li, ZHENG Jingjing, and NING Tigang

Key Laboratory of All Optical Network and Advanced Telecommunication Network, Ministry of Education, Institute of Lightwave Technology, Beijing Jiaotong University, Beijing 100044, China

(Received 12 October 2021; Revised 25 December 2021)

©Tianjin University of Technology 2022

For the PANDA ring-core polarization-maintaining few-mode fiber (RC-PM-FMF) with the given supported eigenmodes, the minimum effective refractive index difference $\min(\Delta n_{\text{eff}})$ between the adjacent eigenmodes decreases with the RC size. Consequently, we propose a PANDA RC-PM-FMF assisted by a ring-sector (RS) structure, which can be used to mainly increase the Δn_{eff} values between the adjacent even and odd eigenmodes with the same polarization. The RS-RC-PM-FMF with an appropriate choice of the parameters can support 10 linearly polarized (LP) eigenmodes, which have $\min(\Delta n_{\text{eff}})$ values higher than 1.9×10^{-4} for the adjacent eigenmodes over the whole C + L band. Furthermore, the fiber is characterized by the low group velocity dispersion (GVD) (-40 — 20 ps \cdot nm $^{-1}$ \cdot km $^{-1}$) and effective mode areas (63 — 104 μm^2), while the total losses are within the range of 0.19 — 0.23 dB/km over the whole band.

Document code: A **Article ID:** 1673-1905(2022)06-0366-6

DOI <https://doi.org/10.1007/s11801-022-1161-3>

With the explosive growth of network traffic, the current optical networks and data centers based on the traditional single-mode fibers (SMFs) are rapidly reaching their maximum capacity. Consequently, various techniques were proposed to overcome the capacity limit, among which space division multiplexing (SDM) has attracted considerable attention in recent years^[1]. First, the SDM system can be realized by using the weakly-coupled multicore fibers (MCFs)^[2], where the elimination of core-to-core crosstalk can allow treating each core as a separate transmission channel. Second, the SDM system based on mode-division multiplexing (MDM) had been demonstrated by means of the single core few-mode fibers (FMFs), in which each mode represents one transmission channel^[3]. However, the FMFs are sensitive to mode coupling, which mainly results from variations of the index distribution along the fiber caused by the fiber manufacturing process as well as by micro and macro bending of the fiber. Although the multiple-input multiple-output (MIMO) digital signal processing (DSP) can be applied to undo the mode-coupling-induced crosstalk and recover data at the receiver, the computational complexity of DSP and cost for MIMO largely increase with the differential group delay (DGD) and mode numbers.

MDM system based on weakly-coupled FMFs can provide a promising solution to this dilemma because they are less dependent on MIMO process. Generally, the weakly-coupled FMFs can be classified into two categories known as the non-polarization-maintaining

(non-PM) and PM FMFs. In the former case, the weakly coupled FMFs supporting four and seven linearly polarized (LP) non-degenerated modes were demonstrated through design modifications with an ring core (RC)^[4] and ring-assisted step-index core^[5], respectively. In the latter case, the effective index difference between two-fold degenerate LP modes of orthogonal polarizations in the PM-FMFs can be increased beyond 1×10^{-4} by introducing stress- and geometry-induced birefringence. Various PM-FMFs have been proposed, such as the highly elliptical core fiber^[6], elliptical ring core (ERC) fiber^[7], ERC fibers assisted by air-holes inside or outside the ERC, PANDA-type fibers with an RC^[8] or ERC^[9], and bow-tie ERC fiber.

In this paper, a PANDA ring-core polarization-maintaining few-mode fiber (RC-PM-FMF) with an improved core design is proposed to increase the effective index difference between adjacent spatial modes. The fiber parameters can be designed by investigating their influences on the mode number and $\min(\Delta n_{\text{eff}})$. Then the fiber properties with the optimal parameters are presented. The cross sections and refractive index profiles of the RC-PM-FMF and the proposed ring-sector (RS)-RC-PM-FMF are shown in Fig.1. The fiber parameters are the inner and outer radii of the RC, r_1 and r_2 , the gap between the RC and circular stress-applying part (SAP) a , the SAP radius r_3 , the RS width and angle, d and θ_s , the gap between the RC and RS b , and the RS rotation-angle from the x -axis θ_r , respectively. When the central line of

* This work has been supported by the National Key Research and Development Program of China (No.2018YFB1801003), and the National Natural Science Foundation of China (No.61575018).

** E-mail: chcwang@bjtu.edu.cn

the RS is parallel to the y -axis, θ equals 90° . The refractive indices of cladding, RC, RS and SAP are represented by n_1, n_2, n_3 and n_4 , respectively. The fiber cladding diameter is $125 \mu\text{m}$. Compared with the former, the feature of the latter is to introduce a pair of RSs (green region) around the RC for increasing the effective index difference between the adjacent spatial eigenmodes, especially to separate the odd and even eigenmodes with the same order and polarization, while the orthogonally polarized modes are mainly split by the stress-induced birefringence.

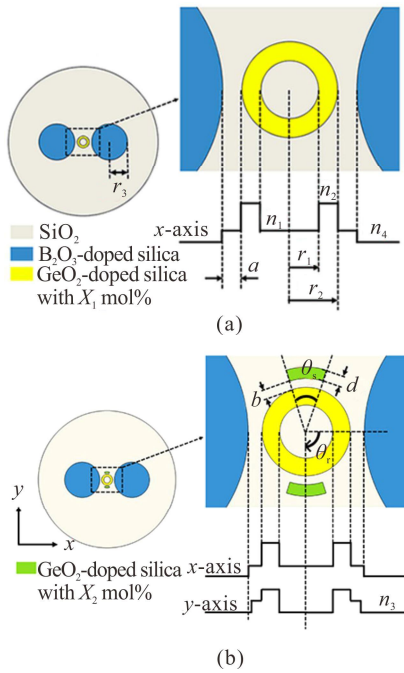


Fig.1 Cross sections and refractive index profiles of (a) the PANDA RC-PM-FMF and (b) RS-RC-PM-FMF

In the simulation, the refractive indices of pure SiO_2 , GeO_2 - and B_2O_3 -doped SiO_2 can be calculated by the Sellmeier equations at different molecular fractions and wavelengths^[10]. The B_2O_3 -doped concentration in SAPs is taken to be 20 mol% in the following discussion, which has been utilized in the practical fabrication. The effective indices and modal field distributions of the guided modes in the PM-FMF can be obtained by numerically solving the wave equations with the COMSOL software based on the full-vector finite element method. The elastic material parameters are presented in Tab.1, including thermal expansion coefficient (α), Young's modulus (E), Poisson's ratio (ν), density (ρ), first and second stress optical coefficients (B_1, B_2), and operating and reference temperature, where the thermal expansion coefficient of a doped material can be obtained using a mixture model as follows

$$\alpha = (1-m)\alpha_0 + m\alpha_1, \quad (1)$$

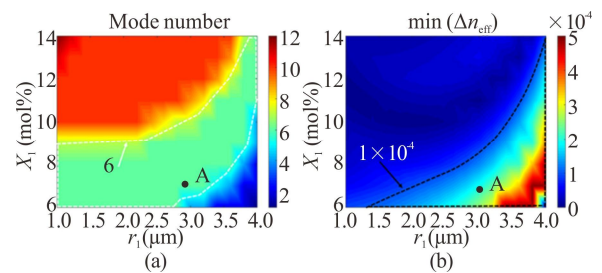
where m indicates the mole percentage of the doping material, and α_0 and α_1 are the thermal expanding coefficients of the background material and the doped material,

respectively. The α_0 of SiO_2 is $5.4 \times 10^{-7} \text{ K}^{-1}$. The α_1 values of GeO_2 and B_2O_3 are $7 \times 10^{-6} \text{ K}^{-1}$ and $10 \times 10^{-6} \text{ K}^{-1}$, respectively.

Tab.1 Elastic parameters used for modeling

	SiO_2	$\text{SiO}_2\text{-GeO}_2$ core	$\text{SiO}_2\text{-B}_2\text{O}_3$ SAPs
Thermal expansion coefficient α (1/K)	5.4×10^{-7}	1.3×10^{-6}	2.4×10^{-6}
Young's modulus E (Pa)	7.3×10^{10}	6.6×10^{10}	4.2×10^{10}
Poisson's ratio ν	0.186	0.177	0.240
Density ρ (kg/m^3)	2196	2354	2254
First stress optical coefficient B_1 (m^2/N)		6.9×10^{-13}	
Second stress optical coefficient B_2 (m^2/N)		4.19×10^{-12}	
Operating temperature ($^\circ\text{C}$)		20	
Reference temperature ($^\circ\text{C}$)		1100	

In order to determine the geometric dimensions and GeO_2 doping concentrations of the RC-PM-FMF and RS-RC-PM-FMF, the mode number and minimum effective refractive index difference $\min(\Delta n_{\text{eff}})$ at 1550 nm are shown in Fig.2. Although the high refractive index contrast between core and cladding combined with small core size can lead to a large $\min(\Delta n_{\text{eff}})$, the absorption loss of the GeO_2 -doped silica increases with the concentration X_1 , while the nonlinear parameter of the fiber increases with a decrease of core diameter. Consequently, the outer radius of the RC r_2 is taken to be $5 \mu\text{m}$ for obtaining a relatively large effective mode area, while the values of X_1 and r_1 are varied from 6 mol% to 14 mol% with $1 \mu\text{m}$ spacing and from $1 \mu\text{m}$ to $4 \mu\text{m}$ with $0.2 \mu\text{m}$ spacing, respectively. One can see that the mode numbers increase with X_1 and decrease with r_1 in the two cases. As shown in Figs.2(a) and (b), the RC-PM-FMF with $X_1=7 \text{ mol\%}$ and $r_1=3 \mu\text{m}$ at the point A can support 6 modes and has a $\min(\Delta n_{\text{eff}})$ value of 1.9×10^{-4} , which is larger than the typical value of 1×10^{-4} between the adjacent eigenmodes. However, a further increase of the mode number for the RC-PM-FMF leads to the $\min(\Delta n_{\text{eff}})$ value lower than 1×10^{-4} . For the RS-RC-PM-FMF, when $X_1=12 \text{ mol\%}$ and $r_1=3 \mu\text{m}$, the $\min(\Delta n_{\text{eff}})$ value can reach 1.4×10^{-4} shown at the point B in Figs.2(c) and (d), while the corresponding intensity distributions of the eigenmodes are shown in Fig.3. In the following discussion, the RS-RC-PM-FMFs supporting 10 separated LP eigenmodes are analyzed.



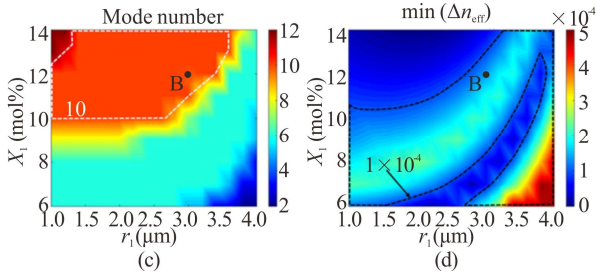


Fig.2 Color maps of the mode number for (a) RC-PM-FMF and (c) RS-RC-PM-FMF and $\min(\Delta n_{\text{eff}})$ at 1550 nm between adjacent eigenmodes for (b) RC-PM-FMF and (d) RS-RC-PM-FMF as functions of X_1 and r_1 , where $r_2=5 \mu\text{m}$, $a=2 \mu\text{m}$, $r_3=15 \mu\text{m}$ ($b=1 \mu\text{m}$, $d=1.5 \mu\text{m}$, $\theta_s=36^\circ$, $\theta_r=90^\circ$ and $X_2=4 \text{ mol}\%$ for the RS-RC-PM-FMF)

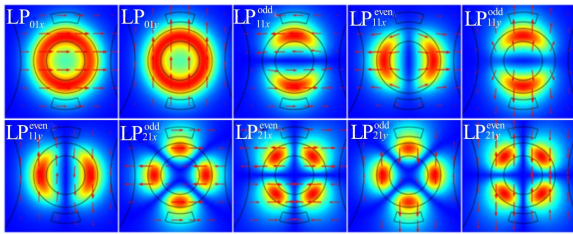


Fig.3 Intensity profiles and electric field polarization directions (red arrows) for the 10 LP eigenmodes at 1550 nm (The superscripts even and odd represent even and odd mode intensity orientations, respectively; The subscripts x and y represent the polarization directions of the electric fields)

According to the condition that the number of modes in the C + L band is equal to 10 and $\min(\Delta n_{\text{eff}})$ between the adjacent eigenmodes is higher than 1×10^{-4} in Figs.2(c) and (d), the values of X_1 and r_1 are taken to be 12 mol%, $3 \mu\text{m}$ and 11 mol%, $2.6 \mu\text{m}$ to calculate the mode number and $\min(\Delta n_{\text{eff}})$ by sweeping the parameters X_2 (from 2 mol% to 6 mol% with 0.5 mol% spacing) and d (from $1 \mu\text{m}$ to $3 \mu\text{m}$ with $0.1 \mu\text{m}$ spacing) at 1550 nm as shown in Fig.4. One can see that the mode number is almost unchanged, indicating the mode number is less dependent on X_2 and d compared with the parameters X_1 and r_1 shown in Fig.2. As shown in Figs.4(b) and (d), when $X_2=5.5 \text{ mol}\%$ and $d=1.3 \mu\text{m}$, the $\min(\Delta n_{\text{eff}})$ values can reach their maximum values of 2×10^{-4} and 1.8×10^{-4} , respectively.

Since the variations of the rotation-angle θ_r and angle θ_s of the RS are related to the intensity distribution of the modes, it is necessary to discuss the influence of these two angles on $\min(\Delta n_{\text{eff}})$. As shown in Fig.5(a), the parameters θ_r (from 60° to 120° with 10° spacing) and θ_s (from 0° to 90° with 9° spacing) are swept to calculate $\min(\Delta n_{\text{eff}})$, while the FMF can maintain supporting 10 eigenmodes. When θ_s is close to 36° , $\min(\Delta n_{\text{eff}})$ can reach its maximum value of 2×10^{-4} at $\theta_r=90^\circ$. The reason is that the RS with a proper choice of parameter θ_s can effectively separate the effective indices between the

even and odd eigenmodes with the same polarization. However, the influence of θ_r on $\min(\Delta n_{\text{eff}})$ is less than that of the θ_s . Tuning rotation angle θ_r symmetrical at $\pm 30^\circ$ on each side of the central line at 90° can lead to a nearly symmetrical variation of $\min(\Delta n_{\text{eff}})$. In Fig.5(b), when $b=1 \mu\text{m}$, $\min(\Delta n_{\text{eff}})$ can reach its maximum value. However, when b is bigger than $1.6 \mu\text{m}$, $\min(\Delta n_{\text{eff}})$ decreases below 1×10^{-4} , which indicates that the distance between the RS and RC should be carefully designed.

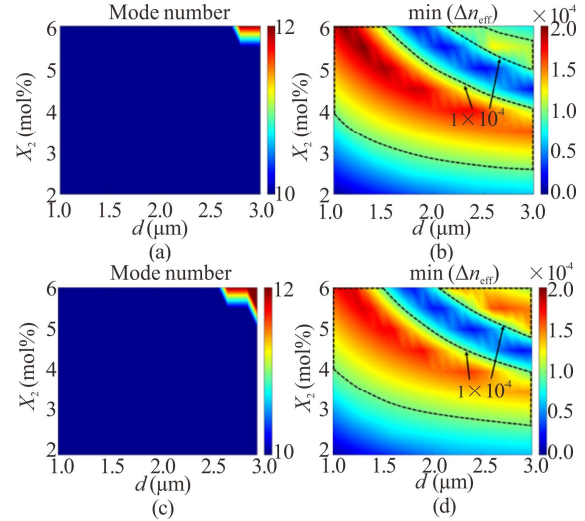
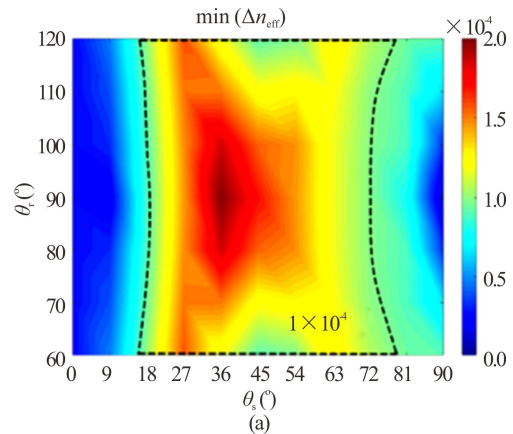


Fig.4 Color maps of the mode number and $\min(\Delta n_{\text{eff}})$ at 1550 nm for the RS-RC-PM-FMF as functions of X_2 and d with (a)(b) $X_1=12 \text{ mol}\%$, $r_1=3 \mu\text{m}$ and (c)(d) $X_1=11 \text{ mol}\%$, $r_1=2.6 \mu\text{m}$, where $r_2=5 \mu\text{m}$, $a=2 \mu\text{m}$, $r_3=15 \mu\text{m}$, $b=1 \mu\text{m}$, $\theta_s=36^\circ$ and $\theta_r=90^\circ$

As the role of the SAPs is mainly to separate the de-generated eigenmodes with orthogonal polarizations, the influence of r_3 and a on $\min(\Delta n_{\text{eff}})$ is presented in Fig.6. The values of r_3 (from $10 \mu\text{m}$ to $20 \mu\text{m}$ with $1 \mu\text{m}$ spacing) and a (from $1 \mu\text{m}$ to $4 \mu\text{m}$ with $0.2 \mu\text{m}$ spacing) are swept to calculate $\min(\Delta n_{\text{eff}})$. The results show that designed RS-RC-PM-FMF can tolerate a large spacing of parameters r_3 and a , where the fiber can satisfy the requirements of $\min(\Delta n_{\text{eff}}) > 1 \times 10^{-4}$ and 10-mode operation. When $r_3=16 \mu\text{m}$ and $a=1.6 \mu\text{m}$, $\min(\Delta n_{\text{eff}})$ can reach its maximum value of 2.3×10^{-4} .



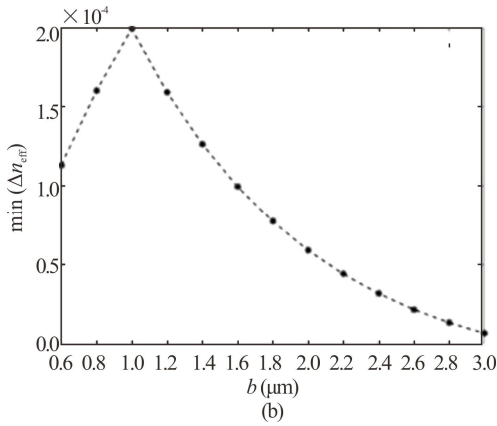


Fig.5 (a) Color map of the $\min(\Delta n_{\text{eff}})$ at 1 550 nm as functions of θ_r and θ_s for the RS-RC-PM-FMF; (b) Curve of $\min(\Delta n_{\text{eff}})$ as a function of b , where $r_1=3 \mu\text{m}$, $r_2=5 \mu\text{m}$, $a=2 \mu\text{m}$, $d=1.3 \mu\text{m}$, $r_3=15 \mu\text{m}$, $b=1 \mu\text{m}$ (only for (a)), $X_1=12 \text{ mol}\%$ and $X_2=5.5 \text{ mol}\%$

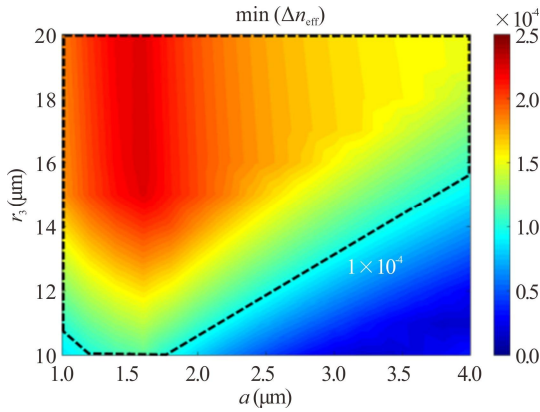


Fig.6 Color map of $\min(\Delta n_{\text{eff}})$ at 1 550 nm as functions of r_3 and a for the RS-RC-PM-FMF, where $r_1=3 \mu\text{m}$, $r_2=5 \mu\text{m}$, $b=1 \mu\text{m}$, $d=1.3 \mu\text{m}$, $X_1=12 \text{ mol}\%$, $X_2=5.5 \text{ mol}\%$, $\theta_s=36^\circ$ and $\theta_r=90^\circ$

Fig.7 shows the effective indices of the 10 eigenmodes in the wavelength range of 1 530—1 630 nm, as well as $\min(\Delta n_{\text{eff}})$ for the RS-RC-PM-FMF with appropriate parameters obtained from the above discussion. As shown in Fig.7(b), the maximum $\min(\Delta n_{\text{eff}})$ of up to 2.3×10^{-4} exists at 1 550 nm, while the minimum value is 1.9×10^{-4} at 1 630 nm. Consequently, the RS-RC-PM-FM with these parameters is analyzed in the following discussion.

Since the group velocity dispersion (GVD) can lead to the temporal broadening of the propagating optical pulses inside the fiber, the GVD profiles with relatively low values are desired for the optical communication systems. The GVD can be calculated by

$$D(\lambda) = -\frac{\lambda}{c} \frac{d^2 n_{\text{eff}}(\lambda)}{d\lambda^2}, \quad (2)$$

where material dispersions of pure silica and Ge-doped silica are taken into account to calculate $n_{\text{eff}}(\lambda)$. The nonlinear effects in the fiber can lead to the spectral broadening and distortion in the pulse shape, which can

be effectively resolved by increasing the effective mode area. The effective mode area A_{eff} is given by

$$A_{\text{eff}} = \frac{\left| \iint |F(x, y)|^2 dx dy \right|}{\iint |F(x, y)|^4 dx dy}, \quad (3)$$

where $F(x, y)$ is the modal intensity distribution of the fiber mode. In Fig.8(a), 10 eigenmodes of the RS-RC-PM-FMF have low and flat GVD profiles, whose values are in the range of -40 — $20 \text{ ps} \cdot \text{nm}^{-1} \cdot \text{km}^{-1}$ over the whole C + L band. The zero dispersion wavelengths of LP_{01} and LP_{11} modes are near $1.5 \mu\text{m}$ and $1.4 \mu\text{m}$, respectively. Moreover, the LP_{21} mode group exhibits a convex-shaped normal GVD profile in the whole wavelength range. Fig.8(b) shows A_{eff} of all eigenmodes higher than $63 \mu\text{m}^2$ over the C + L band.

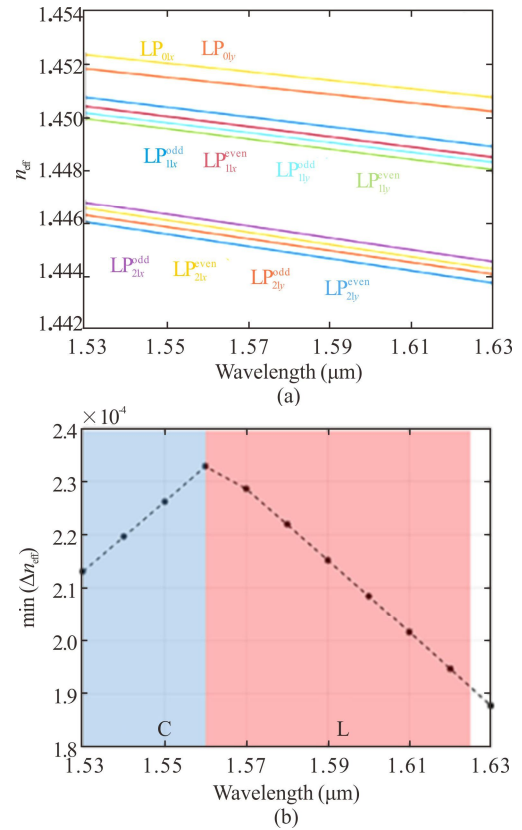


Fig.7 Curves of (a) n_{eff} and (b) $\min(\Delta n_{\text{eff}})$ as a function of wavelength, where $r_1=3 \mu\text{m}$, $r_2=5 \mu\text{m}$, $a=1.6 \mu\text{m}$, $r_3=16 \mu\text{m}$, $b=1 \mu\text{m}$, $d=1.3 \mu\text{m}$, $X_1=12 \text{ mol}\%$, $X_2=5.5 \text{ mol}\%$, $\theta_s=36^\circ$ and $\theta_r=90^\circ$

An equivalent straight fiber with a modified refractive index distribution based on conformal mapping can be used in bending modeling. Tab.2 shows the mode number, $\min(\Delta n_{\text{eff}})$, and maximum bending-induced confinement loss (α_b) under different bend radii along x and y axes. When the bend radius is 5 cm along both two principal axes, the fiber can only support 9 modes because the $\text{LP}_{21y}^{\text{even}}$ mode reaches cut-off state, while the $\max(\alpha_b)$ values are beyond 0.023 dB/km . However, when the bending radius is more than 8 cm along the x and y axes,

the fiber can keep supporting 10 eigenmodes with $\min(\Delta n_{\text{eff}}) > 2.25 \times 10^{-4}$, while the $\max(\alpha_b)$ values are less than 8.45×10^{-4} dB/km and 2.97×10^{-5} dB/km, respectively.

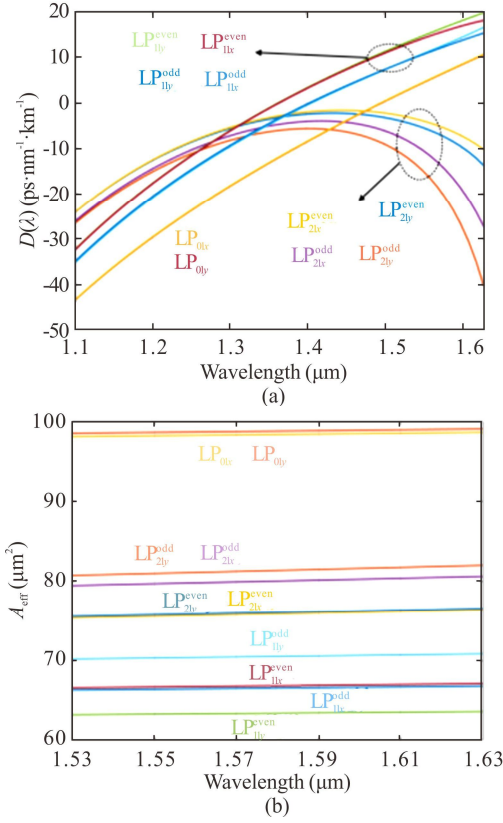


Fig.8 (a) GVD profiles and (b) A_{eff} curves for 10 eigenmodes as a function of wavelength

Tab.2 Mode number, $\min(\Delta n_{\text{eff}})$, and the maximum bending-induced confinement loss under different bend radii and axes at 1 550 nm

Bending radii (cm)		5	6	7	8	15
x-axis	Mode number	9	10	10	10	10
	$\min(\Delta n_{\text{eff}})$ ($\times 10^{-4}$)	2.29	2.28	2.28	2.27	2.27
	$\max(\alpha_b)$ ($\times 10^{-5}$)	0.023	2.130	0.015	84.500	0.052
	Mode number	9	10	10	10	10
	$\min(\Delta n_{\text{eff}})$ ($\times 10^{-4}$)	2.22	2.23	2.24	2.25	2.26
y-axis	$\max(\alpha_b)$ ($\times 10^{-5}$)	0.090	0.004	7.420	2.970	0.115

Furthermore, except for the bending-induced loss, the light wave propagated inside the fiber is attenuated mainly due to Rayleigh scattering^[11], infrared absorption loss^[12] and confinement loss.

As shown in Fig.9(b), all the guided eigenmodes have low losses with L_{total} smaller than 0.23 dB/km over the whole C + L band, while Fig.9(a) shows material losses of pure silica and Ge-doped silica. At 1 550 nm, L_{total} values for LP_{01x} , LP_{01y} , LP_{11x}^{odd} , LP_{11x}^{even} , LP_{11y}^{odd} , LP_{11y}^{even} , LP_{21x}^{odd} , LP_{21x}^{even} , LP_{21y}^{odd} and LP_{21y}^{even} modes are 0.204 dB/km,

0.204 dB/km, 0.207 dB/km, 0.206 dB/km, 0.206 dB/km, 0.207 dB/km, 0.203 dB/km, 0.201 dB/km, 0.203 dB/km and 0.2 dB/km, respectively. Low loss is conducive to long-distance transmission of optical signals.

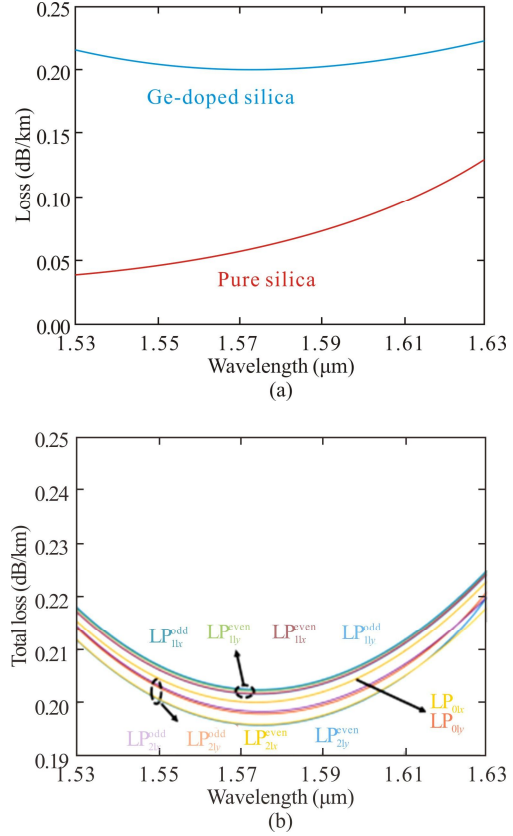
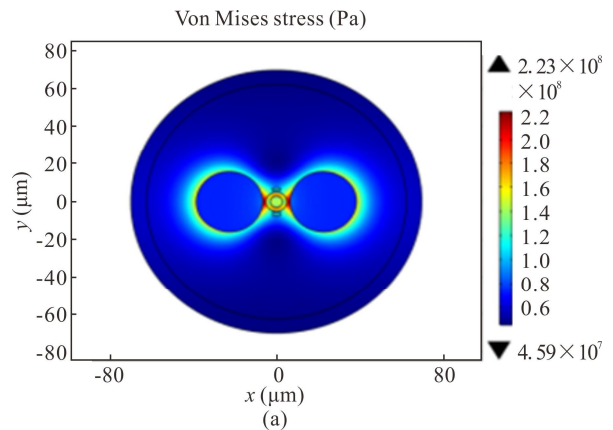


Fig.9 (a) Loss curves for pure silica and Ge-doped silica; (b) Total loss curves of 10 LP modes as a function of wavelength

Fig.10 shows the Von Mises stress distribution and bi-refringence ($B_s = \Delta c(\sigma_x - \sigma_y)$) in the transverse cross-section of the RS-RC-PM-FMF, where $\Delta c = 3.43 \times 10^{-12}$ m²/N, and σ_x and σ_y are the stresses along the x and y directions individually. The region of $B_s > 1 \times 10^{-4}$ is mainly distributed in the middle of the cross-section along the x axis, while the maximum B_s around the core is about 8.54×10^{-4} .



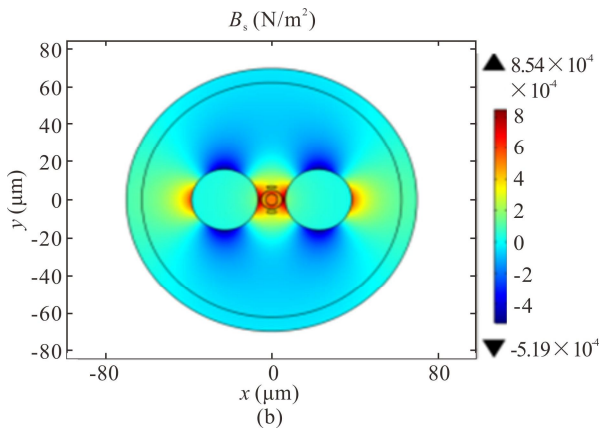


Fig.10 (a) Von Mises stress distribution and (b) stress birefringence distribution in transverse cross section of the RS-RC-PM-FMF at 1550 nm

In conclusion, the RS-RC-PM-FMF, which can fully separate all the 10 LP eigenmodes, is proposed by introducing an RS structure around the center RC. The fiber parameters can be optimized through analyzing their effects on the effective index difference between the adjacent eigenmodes. The RS-RC-PM-FMF with an appropriate choice of parameters can offer $\min(\Delta n_{\text{eff}})$ higher than 1.9×10^{-4} for the adjacent eigenmodes over the whole C + L band. Furthermore, the RS-RC-PM-FMF also has the low GVD (-40 — $20 \text{ ps} \cdot \text{nm}^{-1} \cdot \text{km}^{-1}$), relatively large mode areas (63 — $104 \mu\text{m}^2$) and low total loss (0.19 — 0.23 dB/km), which are beneficial for suppressing the nonlinearity- and dispersion-induced pulse distortions in the spectral and temporal domains and long-distance transmission. Finally, when the bending radius is more than 8 cm along the x and y axes, the bending-induced confinement loss is acceptable and shows its good bending resistance.

The 10-modes PANDA RC-PM-FMF without RS has $\min(\Delta n_{\text{eff}})$ of 1.29×10^{-4} at 1550 nm ^[8], which can be increased to 2.25×10^{-4} for the proposed PM-FMF. The refractive index of RC and the B_2O_3 doping concentration decrease from 1.474 to 1.462 and from 30 mol% to 20 mol%, respectively. As a result, the fiber-fabrication difficulty can be reduced. Moreover, the mode field area of the proposed fiber has an increase because the inner and outer radii of the RC increase from $2 \mu\text{m}$ to $3 \mu\text{m}$, and from $3.8 \mu\text{m}$ to $5 \mu\text{m}$, which is also helpful to minimize the splice loss with the standard single-mode fiber SMF-28.

Statements and Declarations

The authors declare that there are no conflicts of interest related to this article.

References

- [1] RICHARDSON D J, FINI J M, NELSON L E. Space-division multiplexing in optical fibres[J]. *Nature photonics*, 2013, 7(5): 354-362.
- [2] YANG Y, GAO J T, FU S N, et al. Panda type four-core fiber with the efficient use of stress rods[J]. *IEEE photonics journal*, 2019, 11(5): 1-9.
- [3] CORSI A, CHANG J H, WANG R H, et al. Highly elliptical core fiber with stress-induced birefringence for mode multiplexing[J]. *Optics letters*, 2020, 45(10): 2822-2825.
- [4] JUNG Y M, KANG Q Y, ZHOU H Y, et al. Low-loss 25.3 km few-mode ring-core fiber for mode-division multiplexed transmission[J]. *Journal of lightwave technology*, 2017, 35(8): 1363-1368.
- [5] JIANG S L, MA L, ZHANG Z P, et al. Design and characterization of ring-assisted few-mode fibers for weakly-coupled mode-division multiplexing transmission[J]. *Journal of lightwave technology*, 2018, 36(23): 5547-5555.
- [6] CORSI A, CHANG J H, RUSCH L A, et al. Design of highly elliptical core ten-mode fiber for space division multiplexing with 2×2 MIMO[J]. *IEEE photonics journal*, 2019, 11(2): 1-10.
- [7] WANG L X, NEJAD R M, CORSI A, et al. Linearly polarized vector modes: enabling MIMO-free mode-division multiplexing[J]. *Optics express*, 2017, 25(10): 11736-11748.
- [8] YAN H Z, LI S Y, XIE Z Y, et al. Design of PANDA ring-core fiber with 10 polarization-maintaining modes[J]. *Photonics research*, 2017, 5(1): 1-5.
- [9] CHEN S, WANG J. Design of PANDA-type elliptical-core multimode fiber supporting 24 fully lifted eigenmodes[J]. *Optics letters*, 2018, 43(15): 3718-3721.
- [10] FLEMING J W. Dispersion in GeO_2 - SiO_2 glasses[J]. *Applied optics*, 1984, 23(24): 4486-4493.
- [11] LIU Y P, YANG Z Q, ZHAO J, et al. Intrinsic loss of few-mode fibers[J]. *Optics express*, 2018, 26(2): 2107-2116.
- [12] ONISHI M, KASHIWADA T, ISHIGURO Y, et al. High performance dispersion-compensating fibers[J]. *Fiber and integrated optics*, 1997, 16(3): 277-285.